Earthq Eng & Eng Vib (2018) 17: 277-291 **DOI**: https://doi.org/10.1007/s11803-018-0441-1

Hysteretic energy prediction method for mainshock-aftershock sequences

Zhai Changhai[1, 2†], Ji Duofa[1, 2‡], Wen Weiping[1, 2§], Li Cuihua[1, 2‡], Lei Weidong[3*] and Xie Lili[2,4†]

1. *Key Lab of Structures Dynamic Behavior and Control* (*Harbin Institute of Technology*)*, Ministry of Education, Heilongjiang, Harbin 150090, China*
2. *School of Civil Engineering, Harbin Institute of Technology, Harbin 150090, China*
3. *Shenzhen Graduate School, Harbin Institute of Technology, Shenzhen 518055, China*
4. *Institute of Engineering Mechanics, China Earthquake Administration, Harbin 150080, China*

Abstract: Structures located in seismically active regions may be subjected to mainshock-aftershock (MSAS) sequences. Strong aftershocks significantly affect the hysteretic energy demand of structures. The hysteretic energy, $E_{H,seq}$, is normalized by mass m and expressed in terms of the equivalent velocity, $V_{D,seq}$, to quantitatively investigate aftershock effects on the hysteretic energy of structures. The equivalent velocity, $V_{D,seq}$, is computed by analyzing the response time-history of an inelastic single-degree-of-freedom (SDOF) system with a varying vibration period subjected to 309 MSAS sequences. The present study selected two kinds of MSAS sequences, with one aftershock and two aftershocks, respectively. The aftershocks are scaled to maintain different relative intensities. The variation of the equivalent velocity, $V_{D,seq}$, is studied for consideration of the ductility values, site conditions, relative intensities, number of aftershocks, hysteretic models, and damping ratios. The MSAS sequence with one aftershock exhibited a 10% to 30% hysteretic energy increase, whereas the MSAS sequence with two aftershocks presented a 20% to 40% hysteretic energy increase. Finally, a hysteretic energy prediction equation is proposed as a function of the vibration period, ductility value, and damping ratio to estimate hysteretic energy for mainshock-aftershock sequences.

Keywords: hysteretic energy; mainshock-aftershock sequences; SDOF system; relative intensity; prediction equation

1 Introduction

Recent earthquakes suggest strong mainshocks are followed by many aftershocks (CENC, 2008; Kyoshin-Net, 2009). For example, five aftershocks (M_w>6.0) were recorded for the 2008 M_w 7.9 Wenchuan earthquake (CENC, 2008). However, there often is insufficient time to repair mainshock-damaged buildings prior to the occurrence of subsequent aftershocks, thereby further worsening the conditions of mainshock-damaged buildings as confirmed during post-earthquake field reconnaissance (Augenti and Parisi, 2010; Ceci *et al.*, 2010; Di Sarno *et al.*, 2013). Unfortunately, current seismic codes are established on the basis of a single design earthquake and do not consider the aftershocks (CEN, 2003; IBC, 2006). It is therefore of great significance to investigate the effects of mainshock-aftershock (MSAS) sequences on such structures.

Currently, extensive investigations have been conducted to discuss the importance of considering the effects of aftershocks on the inelastic response spectra of single-degree-of-freedom (SDOF) systems (Hatzigeorgiou, 2010a, b; Moustafa and Takewaki, 2011; Goda, 2012; Goda and Taylor, 2012; Di Sarno, 2013; Zhai *et al.*, 2013a, b; Zhai *et al.*, 2014, 2015). Several principles have been proposed to consider the effects of aftershocks in performance-based seismic design. In addition, some studies have exhibited the effects of aftershocks on multiple-degree-of-freedom (MDOF) structures (Hatzigeorgiou and Liolios, 2010; Moustafa and Takewaki, 2010; Ruiz-García and Negrete-Manriquez, 2011; Faisal *et al.*, 2013; Nazari *et al.*, 2013).

Housner (1956) initially proposed the energy method, which was subsequently employed by many investigations (Zahrah and Hall, 1982; Akiyama, 1985; Kuwamura and Galambos, 1989; Uang and Bertero, 1990; Fajfar and Vidic, 1994; Chai *et al.*, 1995, 1998;

Correspondence to: Zhai Changhai, School of Civil Engineering, Harbin Institute of Technology, China
Tel: +86-451-86403564
E-mail: zch-hit@hit.edu.cn
†Professor; ‡PhD Candidate; §Assistant Professor; *Associate Professor

Supported by: National Key R&D Program of China under Grant No. 2017YFC1500602 and 2016YFC0701108, the National Natural Science Foundation of China under Grant No. 51322801 and 51708161, the Outstanding Talents Jump Promotion Plan of Basic Research of Harbin Institute of Technology, China Postdoctoral Science Foundation under Grant No. 2016M601430

Received July 27, 2016; **Accepted** February 12, 2017

Chai and Fajfar, 2000; Zhai *et al*., 2016) to replace conventional design methods. Recent scientific efforts (Decanini and Mollaioli, 1998, 2001; Manfredi, 2001; Riddell and Garcia, 2001; Arroyo and Ordaz, 2007a, b; Dindar *et al*., 2015) have been devoted to interpreting the seismic demand of structures from the perspective of the hysteretic energy demand spectra. Several studies extended the energy method from SDOF systems to MDOF systems (Choi and Kim, 2006; Bojórquez *et al.*, 2008; Bojórquezet *et al.*, 2010; Gong *et al.*, 2012). The equivalent energy velocity has been used in several seismic design codes for the energy spectra design (Benavent-Climent *et al.*, 2002, 2010; Amiri *et al.*, 2008; López-Almansa *et al.*, 2013).

Hysteretic energy and damage simultaneously appear and are caused by the inelastic deformation of structures. Therefore, hysteretic energy can be considered as an effective measure in assessing seismic structural damage. Nevertheless, the effects of aftershocks on hysteretic energy have not been fully investigated. In addition, many studies (Hatzigeorgiou, 2010a, b; Moustafa and Takewaki, 2011; Goda, 2012; Goda and Taylor, 2012; Di Sarno, 2013; Zhai *et al.*, 2013a, b) have noted the prominence of aftershock effects in performance-based seismic design. Therefore, it is of great significance to investigate the characteristics of hysteretic energy in mainshock-aftershock sequences.

In light of the above discussions, the present study evaluated the hysteretic energy of inelastic SDOF structures subjected to MSAS sequences. Three hysteretic models were chosen to represent structures with different inelastic behaviors. The relative intensity (∇ PGA), which is defined as the ratio of the aftershock *PGA* to that of the corresponding mainshock, was used to scale the intensity of the aftershocks. The hysteretic energy of the MSAS sequences was normalized by its mass, *m*, and expressed in terms of the equivalent velocity, $V_{\mathrm{D,seq}}$. Finally, a prediction equation for $V_{\mathrm{D,seq}}$ was proposed through extensive parameter analysis.

2 Definition of energy response parameters

The hysteretic energy of a SDOF system can be expressed as follows (Uang and Bertero, 1990):

$$E_{\mathrm{H}} = \int f_{\mathrm{s}}\mathrm{d}x - (f_{\mathrm{s}})^2 / (2k) \tag{1}$$

where E_{H} is the hysteretic energy, and f_{s} is the resisting force.

In this study, the hysteretic energy is normalized by mass *m* and expressed in terms of the equivalent velocity, V_{D}, which is defined as follows:

$$V_{\mathrm{D}} = \sqrt{2E_{\mathrm{H}} / m} \tag{2}$$

Dindar *et al.* (2015) investigated the relation between hysteretic energy, E_{H}, and PGA, as follows:

$$E_{\mathrm{H}} = \left(PGA / 0.1\mathrm{g}\right)^2 \times E_{\mathrm{H}}^{0.1\mathrm{g}} \tag{3}$$

where *PGA* is the peak ground acceleration of the ground motions and $E_{\mathrm{H}}^{0.1\mathrm{g}}$ is the hysteretic energy for a *PGA* of 0.1 g. The relation between the equivalent velocity, V_{D}, and *PGA* of the ground motions can be deduced from Eqs. (2) and (3) as follows:

$$V_{\mathrm{D}} = \left(PGA / 0.1\mathrm{g}\right) \times V_{\mathrm{D}}^{0.1\mathrm{g}} \tag{4}$$

where $V_{\mathrm{D}}^{0.1\mathrm{g}}$ is the equivalent velocity for a *PGA* of 0.1 g. Equation (4) is suitable for the relation between the equivalent velocity, V_{D}, and *PGA* for structures under single ground motions.

The aftershocks were scaled for different intensities to investigate the effects of aftershocks on hysteretic energy. The notation ∇PGA is introduced and is defined as the ratio of the *PGA* of the aftershock, PGA_{as}, to that of the corresponding mainshock, PGA_{ms}, as follows:

$$\nabla PGA = PGA_{\mathrm{as}} / PGA_{\mathrm{ms}} \tag{5}$$

The *PGA* of aftershocks can be written as follows:

$$PGA_{\mathrm{as}} = \nabla PGA \times PGA_{\mathrm{ms}} \tag{6}$$

From Eqs. (4) and (6), the equivalent velocity of the mainshocks and aftershocks, respectively, can be expressed as follows:

$$V_{\mathrm{D,ms}} = \left(PGA_{\mathrm{ms}} / 0.1\mathrm{g}\right) \times V_{\mathrm{D,ms}}^{0.1\mathrm{g}} \tag{7}$$

$$V_{\mathrm{D,as}} = \left(\nabla PGA \times PGA_{\mathrm{ms}} / 0.1\mathrm{g}\right) \times V_{\mathrm{D,as}}^{0.1\mathrm{g}} \tag{8}$$

where $V_{\mathrm{D,ms}}$ is the equivalent velocity of the mainshocks, $V_{\mathrm{D,ms}}^{0.1\mathrm{g}}$ is the equivalent velocity of the mainshocks for a PGA_{ms} of 0.1 g, $V_{\mathrm{D,as}}$ is the equivalent velocity of the aftershocks, and $V_{\mathrm{D,as}}^{0.1\mathrm{g}}$ is the equivalent velocity of the aftershocks for a PGA_{as} of 0.1 g.

The equivalent velocity of the MSAS sequences is described as follows:

$$\begin{aligned} V_{\mathrm{D,seq}}^{PGA_{\mathrm{ms}}} &= \left(PGA_{\mathrm{ms}} / 0.1\mathrm{g}\right) \times V_{\mathrm{D,ms}}^{0.1\mathrm{g}} + \left(\nabla PGA \times PGA_{\mathrm{ms}} / 0.1\mathrm{g}\right) \times V_{\mathrm{D,as}}^{0.1\mathrm{g}} \\ &= \left(PGA_{\mathrm{ms}} / 0.1\mathrm{g}\right)\left(V_{\mathrm{D,ms}}^{0.1\mathrm{g}} + \nabla PGA \times V_{\mathrm{D,as}}^{0.1\mathrm{g}}\right) \end{aligned} \tag{9}$$

If an MSAS sequence with a PGA_{ms} has a value equal to 0.1 g, then the PGA_{as} of the MSAS sequence would equal $\nabla PGA \times 0.1$ g. According to Eq. (4), the equivalent velocity of the mainshock with a PGA_{ms} of 0.1 g and an aftershock with a PGA_{as} of $\nabla PGA \times 0.1$ g, respectively, can be written as follows:

$$V_{\mathrm{D,ms}} = \left(0.1\mathrm{g} / 0.1\mathrm{g}\right) \times V_{\mathrm{D,ms}}^{0.1\mathrm{g}} = V_{\mathrm{D,ms}}^{0.1\mathrm{g}} \tag{10}$$

$$V_{\mathrm{D,as}} = \left(\nabla PGA \times 0.1\mathrm{g} / 0.1\mathrm{g}\right) \times V_{\mathrm{D,as}}^{0.1\mathrm{g}} = \nabla PGA \times V_{\mathrm{D,as}}^{0.1\mathrm{g}} \quad (11)$$

Thus, the equivalent velocity of this MSAS sequence can be written as follows:

$$V_{\mathrm{D,seq}}^{0.1\mathrm{g}} = V_{\mathrm{D,ms}}^{0.1\mathrm{g}} + \nabla PGA \times V_{\mathrm{D,as}}^{0.1\mathrm{g}} \quad (12)$$

where $V_{\mathrm{D,seq}}^{0.1\mathrm{g}}$ is the equivalent velocity of the MSAS sequences for a PGA_{ms} of 0.1 g.

According to Eqs. (9) and (12), the equivalent velocity of MSAS sequences can be written as follows:

$$V_{\mathrm{D,seq}}^{PGA_{\mathrm{ms}}} = \left(PGA_{\mathrm{ms}} / 0.1\mathrm{g}\right) V_{\mathrm{D,seq}}^{0.1\mathrm{g}} \quad (13)$$

Therefore, the present study may proceed with the use of Eq. (4) for the examined MSAS sequences used in this study, where the energy terms were computed in terms of the unit mass.

The present study employed three hysteretic models: (i) elastic-perfectly-plastic (EPP) model, which represents a non-degrading system; (ii) modified-clough (MC) model, which simulates the flexural behavior and exhibits stiffness degradation upon reloading (Miranda and Ruiz-Garcia, 2002; Zhai *et al.*, 2013b); and (iii) stiffness strength degradation (SSD) model based on the three-parameter model (Kunnath *et al.*, 1990; Kunnath *et al.*, 1992), which represents the global behavior of systems that exhibit stiffness degradation and strength deterioration during reloading branches. Moreover, Figure 1 presents the force-displacement loops for these three models, which were obtained from the time history analysis of a SDOF structure subjected to an MSAS sequence with one aftershock (M_{w}=5.9) that was recorded in the Chi-Chi earthquake (TCU067 N-S).

The present study evaluated inelastic SDOF systems with a set of 79 vibration periods (a period range of 0.1 s–2.0 s with a time-step of 0.05 s and a period range of 2.0 s–6.0 s with a time-step of 0.1 s). Three viscous damping ratios (ζ = 0.02, 0.05, and 0.1) were adopted. Five ductility values (μ = 2, 3, 4, 5, and 6) were considered to investigate different ductility performances. The ductility value is defined as follows:

$$\mu = \frac{x_{\mathrm{m}}}{x_{\mathrm{y}}} \quad (14)$$

where x_{m} is the maximum relative displacement of a SDOF system, and x_{y} is the yield displacement of a SDOF system.

Figure 2 illustrates the computation flowchart of hysteretic energy. c, K_0, w_{n}, F_{e}, x_{e}, and $V_{\mathrm{D,ms}}$ represent the damping coefficient, elastic stiffness, natural circular frequency, maximum elastic force, maximum elastic displacement, and equivalent velocity of the mainshocks, respectively. The hysteretic energy was calculated by gradually reducing the applied strength of the SDOF systems from the corresponding elastic strength demand until a specified ductility value with a tolerance of 1% was achieved.

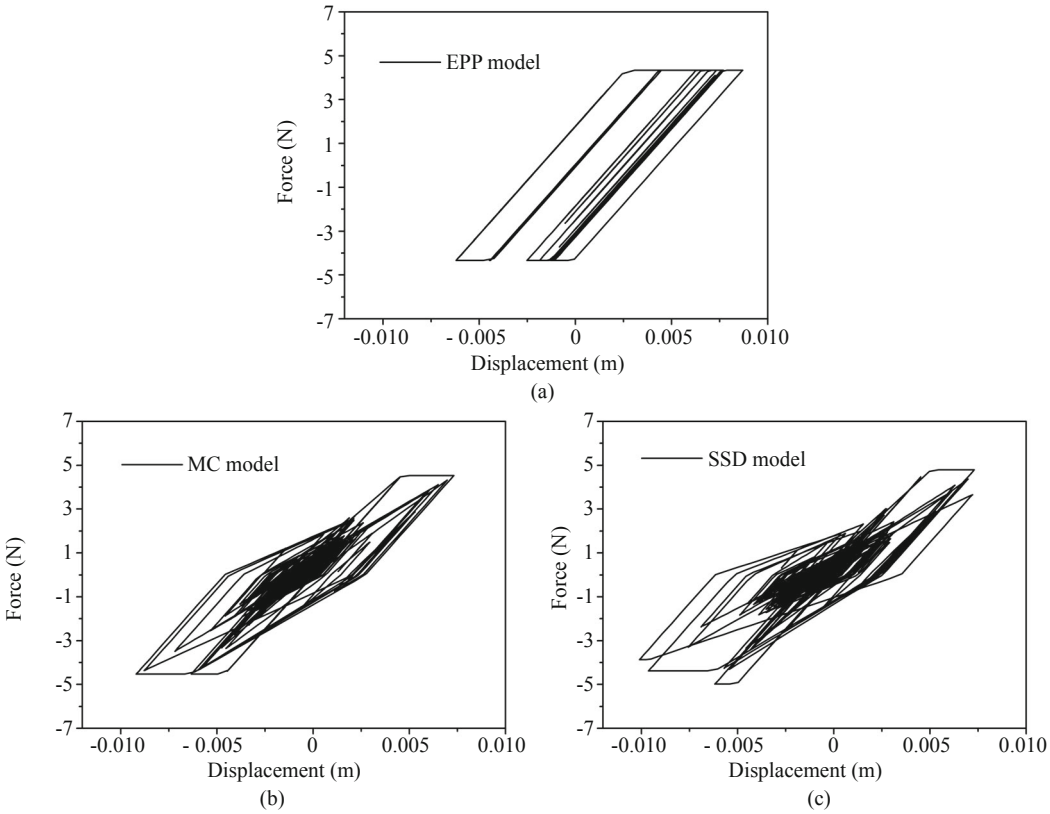

Fig. 1 Force–displacement loops of SDOF structures under a set of given conditions (for Chi-Chi earthquake sequence including one aftershock M_{w} = 5.9, ζ = 0.05, ∇PGA = 0.8, μ = 2 and T = 0.2 s), for three models: (a) EPP; (b) MC; (c) SSD

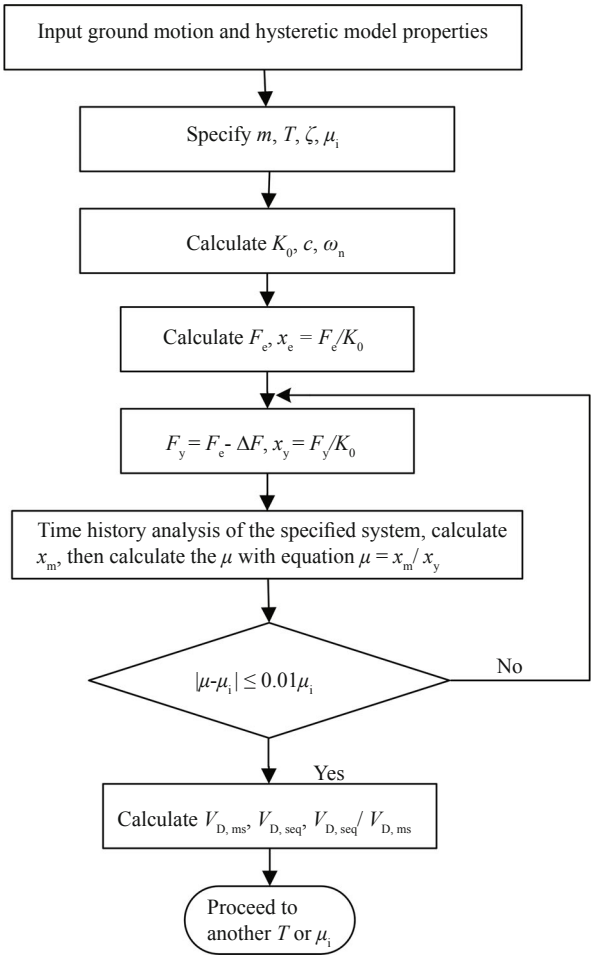

Fig. 2 Computation flowchart of hysteretic energy

3 Ground motions

The present study evaluated two kinds of MSAS sequences, with one aftershock and two aftershocks, respectively. The site classification in this study adopted the definitions of the USGS site classification system (Boore, 1993). The number of qualified MSAS sequences recorded for site classes A and D was not included in this manuscript as they are limited.

Many researchers (Baker and Allin, 2006; Baker, 2010; Katsanos *et al.*, 2010; Ay and Akkar, 2012) proposed the criteria for selecting single earthquake ground motions, though these criteria are not applicable for selecting MSAS sequences given the limited number of MSAS sequences. Therefore, MSAS sequences were selected from the earthquake database in such a way that (1) there is sufficient geological and geotechnical information at the recording station, where an acceleration device was located; (2) the ground motion was recorded at a free field station, or on the ground level of a building; (3) for sequences with one aftershock, the *PGA* of the mainshocks and aftershocks are both greater than 0.1 g; and (4) for sequences with two aftershocks, the *PGA* of the mainshocks is greater than 0.1 g, and the *PGA* of every individual aftershock is greater than 0.05 g. Tables 1 and 2 present the selected MSAS sequences for the present study, specifically a total of 218 recorded MSAS sequences with one aftershock and a total of 91 recorded MSAS sequences with two aftershocks. The MSAS sequences were obtained from the PEER NGA database (http://ngawest2.berkeley.edu/). The present study applied a time gap of 100 s between two consecutive ground motions to simulate a real situation (Hatzigeorgiou, 2010a; Moustafa and Takewaki, 2011; Zhai *et al.*, 2013a, b; Zhai *et al.*, 2014, 2015).

For MSAS sequences with one aftershock, aftershocks with $\nabla PGA < 0.5$ presented slight influences on the structural response (Zhai *et al.*, 2013a). Thus, $\nabla PGA = 0.5$ was employed as the smallest relative intensity. Although cases that exhibited a larger aftershock *PGA* than that of the corresponding mainshock have been recorded in the Chi-Chi earthquake (Zhai *et al.*, 2013a), it is a rare phenomenon. Therefore, $\nabla PGA = 1.0$ was employed to simulate the extreme case, while $\nabla PGA = 0.8$ (Zhai *et al.*, 2013a; Dong and Frangopol, 2015) was considered as a moderate aftershock.

The intensities of aftershocks are dependent on earthquake magnitude, rupture distance, and site condition. Thus MSAS sequences with two aftershocks generally present different aftershock intensities and vary significantly with changes in magnitude, rupture distance, and site condition. In order to simplify the situation, two aftershocks were scaled to the same intensity. $\nabla PGA = 0.5$ was used as the smallest relative intensity. Hatzigeorgiou (2010b) repeated a seed record component with a scaling factor of 0.8526 to construct an MSAS sequence with three seismic events. According to Goda (2012), the method may induce bias towards the evaluation of the seismic demand. Therefore, $\nabla PGA = 0.8$ was used to simulate the extreme case.

A sequence with two aftershocks recorded in the Chi-Chi earthquake (CHY046 W-E) was selected to demonstrate the aftershock effects on hysteretic energy. The *PGA* of the mainshock, first aftershock, and second aftershock are equal to 0.1424 g, 0.1204 g and 0.1012 g, respectively. Figure 3 (a) presents the ratio of the hysteretic energy for the sequence with one aftershock to that of the corresponding mainshock. Figure 3 (b) illustrates the ratio of the hysteretic energy for the sequence with two aftershocks to that of the corresponding mainshock. Figure 3 indicates that the sequence with one aftershock can increase the hysteretic energy by 15%, whereas the sequence with two aftershocks presented a hysteretic energy incremental percentage increase of 40%. Therefore, research on the effects of aftershocks on hysteretic energy is necessary.

4 Influence of various factors on $V_{D,seq}$

4.1 Mean $V_{D,seq}$

A total of 1,098,495 hysteretic energy indices, specifically 309 MSAS sequences, 79 vibration periods,

Table 1 Seismic information of MSAS sequences with one aftershock and the number of ground motions

Earthquake name	Mainshock		Aftershock		Number of ground motions	
	Time	M_W	Time	M_W	Site Class B	Site Class C
Imperial Valley	1979-10-15,23:16	6.53	1979-10-15, 23:19	5.01	0	19
Northridge	1994-01-17,12:31	6.69	1994-01-17, 12:32	6.05	1	8
			1994-03-20, 21:20	5.28	13	19
ChiChi	1999-09-20	7.62	1999-09-20, 17:57	5.9	7	3
			1999-09-20, 18:03	6.2	32	8
			1999-09-20, 21:46	6.2	15	6
			1999-09-20, 00:14	6.2	18	24
			1999-09-20, 23:52	6.3	30	15

Table 2 Seismic information of MSAS sequences with two aftershocks and the number of ground motions

ChiChi Mainshock		1st Aftershock		2nd Aftershock		Number of ground motions	
Time	M_W	Time	M_W	Time	M_W	Site Class B	Site Class C
1999-9-20	7.62	1999-09-20, 17:57	5.9	1999-09-20, 18:03	6.2	3	4
				1999-09-20, 21:46	6.2	0	2
				1999-09-22, 00:14	6.2	1	1
				1999-09-25, 23:52	6.3	2	0
		1999-09-20, 18:03	6.2	1999-09-20, 21:46	6.2	6	2
				1999-09-22, 00:14	6.2	11	6
				1999-09-25, 23:52	6.3	12	0
		1999-09-20, 21:46	6.2	1999-09-22, 00:14	6.2	2	2
				1999-09-25, 23:52	6.3	5	4
		1999-09-22, 00:14	6.2	1999-09-25, 23:52	6.3	14	14

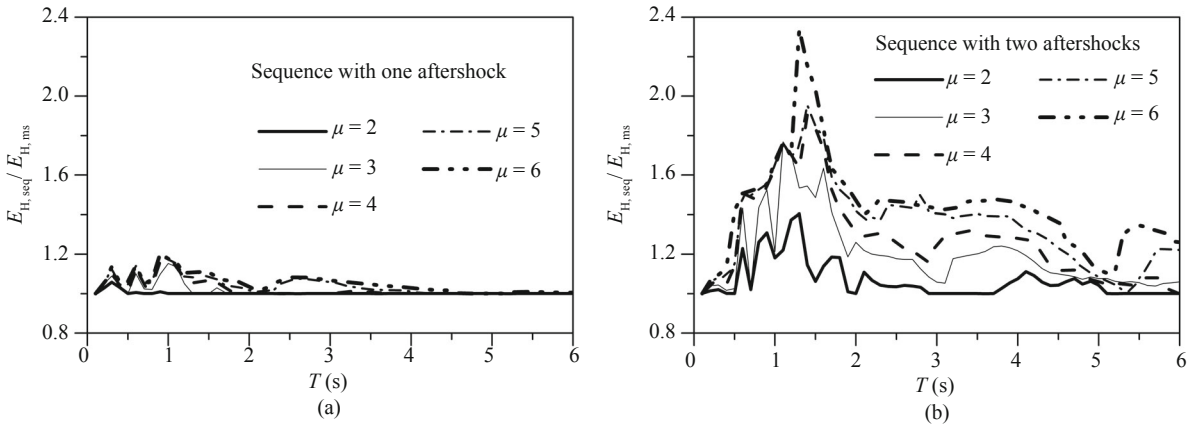

Fig. 3 Ratios of hysteretic energy between sequence and mainshock for sequence recorded in Chi-Chi earthquake (CHY046 W-E): (a) sequence with one aftershock; (b) sequence with two aftershocks

five levels of ductility values, and three levels of relative intensities, for the three hysteretic models were computed as a part of this investigation. The result of each period, each ductility value, each relative intensity value, and each local site condition were then averaged to calculate the mean hysteretic energy indices. Note that for the brevity of the paper, MSAS sequences with one aftershock were used to study $V_{D,seq}$ in the following sections except Section 4.4. The seismic sequences effects on $V_{D,seq}$ were investigated using MSAS sequences with one aftershock and two aftershocks in Section 4.4. The mainshock in the MSAS sequences was scaled to 0.1 g. The short, medium, and long period ranges were 0 s–0.5 s, 0.5 s–1.5 s, and 1.5 s–6 s, respectively.

Figure 4 presents the variation of the mean $V_{D,seq}$ for the EPP systems under a set of given conditions (for MSAS sequences with one aftershock, $\zeta = 0.05$, $\nabla PGA = 0.5$ and $m = 2$, 3, 4, 5, and 6) at two different site classes. In the

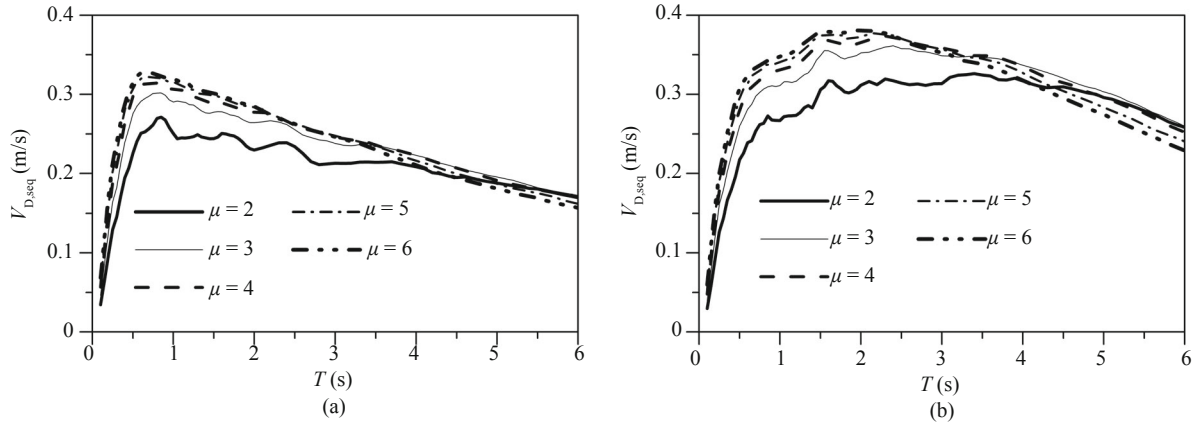

Fig. 4 Mean $V_{D,seq}$ for the EPP systems under a set of given conditions (for MSAS sequences with one aftershock, ζ = 0.05, ∇ *PGA* = 0.5 and μ = 2, 3, 4, 5 and 6) at two different site classes: (a) Site B; (b) Site C

short period range, the mean $V_{D,seq}$ increased following an increase in vibration period. In the medium-long period range, the mean $V_{D,seq}$ was moderately dependent on the vibration period and exhibited a slow increase with an increase in vibration period. In the long period range, the mean $V_{D,seq}$ was dependent on the vibration period and presented a decrease with an increase of the vibration period.

The critical period was introduced to define different variations of the mean $V_{D,seq}$ versus vibration period. For example, structures built on site classes B and C exhibited a rough constant of 0.5 s for the first critical period, wherein the ductility value increased from 2 to 6 (Fig. 4). The mean $V_{D,seq}$ in site class B exhibited a second critical period decrease from 0.90 s to 0.65 s as the ductility value increased from 2 to 6, as presented in Fig. 4 (a).

For the whole period, the mean $V_{D,seq}$ was dependent on and increased with the ductility value, μ, except ductility values μ =2 and μ =3 in the long period range. Structures built on site class C exhibited a mean $V_{D,seq}$ increase from 0.22 to 0.30 as the ductility value, μ, increased from 2 to 6 at a vibration period of T = 0.5 s. Likewise, the mean $V_{D,seq}$ increased from 0.31 to 0.38 as the ductility value, μ, increased from 2 to 6 at a vibration period of T = 2 s.

4.2 Variability of $V_{D,seq}$

The coefficient of variation is denoted as COV and reflects the relative dispersion of a series of numbers. Figure 5 illustrates the COV variation of $V_{D,seq}$ for the EPP systems under a set of given conditions (for MSAS sequences with one aftershock, ζ = 0.05, ∇ *PGA* = 0.5, and μ = 2, 3, 4, 5, and 6) at two different site classes.

The variation of COV in Fig. 5 presents a similar general trend regardless of site conditions. The COV varied from 0.2–0.3 to 0.8–0.9 in the period range, which is meaningful for engineering structures. The largest value of COV (1.02) corresponds to a ductility value, μ, of 2 in Fig. 5 (b). The ductility value, μ, did not present any significant effect on the COVs in the short period range. By contrast, the differences among the COVs for different ductility values, μ, gradually enlarged as the vibration period increased. The COVs were significantly dependent on the variation period for the whole period

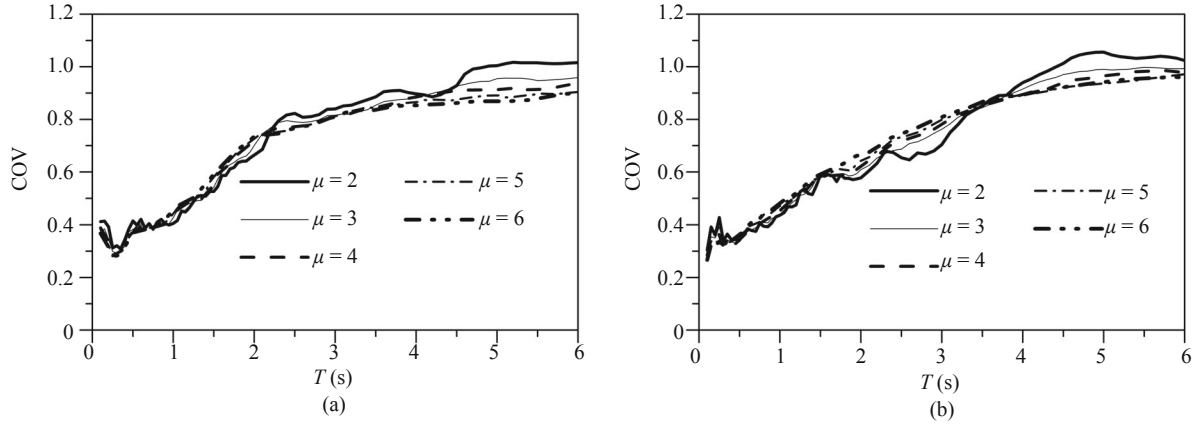

Fig. 5 COVs of $V_{D,seq}$ for the EPP systems under a set of given conditions (for MSAS sequences with one aftershock, ζ = 0.05, ∇ *PGA* = 0.5 and μ = 2, 3, 4, 5 and 6) at two different site classes: (a) Site B; (b) Site C

range as they exhibited increases with an increase in the vibration period.

4.3 Effect of soil condition

An error may have been produced as the mean $V_{D,seq}$ of a specific site class was evaluated using the mean $V_{D,seq}$ of all site classes. The results in Fig. 6 provide assessment measurements for errors generated by ignoring the influence of specific site conditions. The mean $V_{D,seq}$ of a given site in Fig. 6 was normalized by the mean $V_{D,seq}$ of all the site classes for the EPP systems under a set of given conditions (for MSAS sequences with one aftershock, $\zeta = 0.05$, $\nabla PGA = 0.5$ and $\mu = 2$, 3, 4, 5, and 6). $V_{D,B}$ and $V_{D,C}$ represent the mean $V_{D,seq}$ of site classes B and C, respectively. $V_{D,BC}$ represents the mean $V_{D,seq}$ of all site classes.

In general, the $V_{D,B}/V_{D,BC}$ ratios in Fig. 6 (a) were greater than 1.0 in the short period range, which indicates the production of an underestimation error when the mean $V_{D,seq}$ of site class B was evaluated using the mean $V_{D,seq}$ of all site classes. The $V_{D,C}/V_{D,BC}$ ratios (<1) in the short period range in Fig. 6 (b) indicate an overestimation error when the $V_{D,seq}$ of site class C was evaluated using the mean $V_{D,seq}$ of all site classes. Structures with long periods presented a high level of underestimation or overestimation of 25%, which may have been caused by resonance with the soil. Therefore, the effects of the site conditions could not be neglected in the long period range. However, the ratios in Fig. 6 are approximately close to 1.0 in the short-medium period range, thereby suggesting a low level of underestimation or overestimation of 6%. Thus, the effects of the site conditions on the $V_{D,seq}$ could be reasonably neglected in the short-medium period range.

4.4 Effect of relative intensity and number of aftershocks

The ratios of V_D for the MSAS sequences to that for the corresponding mainshock were calculated for each MSAS sequence, each vibration period, each ductility value, and each relative intensity value to study the effects of aftershocks on V_D. The equivalent velocity for the MSAS sequences and for the corresponding mainshock are denoted as $V_{D,seq}$ and $V_{D,ms}$, respectively.

Figure 7 presents the variation of the mean $V_{D,seq}/V_{D,ms}$ for the EPP systems under a set of given conditions (for MSAS sequences with one aftershock on site class B, $\zeta = 0.05$ and $\mu = 2$, 3, 4, 5, and 6) for different relative intensities. Figure 7 presents a mean $V_{D,seq}/V_{D,ms}$ greater than 1.0, which indicates an aftershock-caused increase in V_D. The mean $V_{D,seq}/V_{D,ms}$ in Fig. 7 (a) is roughly less than 1.05 and is almost independent of the vibration period. Figures 7 (b) and (c) exhibited a mean $V_{D,seq}/V_{D,ms}$ of around 1.1 and 1.15, respectively.

As the relative intensity, ∇PGA, increased from 0.5 to 1.0, the effects of the aftershocks on V_D generally increased from 5% to 15% for most of the vibration periods. The effects of the aftershocks on the hysteretic energy in Fig. 7 presented an increase from 10% to 30% as the relative intensity, ∇PGA, increased from 0.5 to 1.0.

The mainshock-damaged structure is generally subjected to several aftershocks. Thus, the effects of MSAS sequences with two aftershocks on V_D were investigated. Figure 8 illustrates the variation of the mean $V_{D,seq}/V_{D,ms}$ for the EPP systems under a set of given conditions (for MSAS sequences with two aftershocks on site class B, $\zeta = 0.05$ and $\mu = 2$, 3, 4, 5, and 6) for different relative intensities.

Figures 7 and 8 present a mean $V_{D,seq}/V_{D,ms}$ that demonstrates similar trends. The results in Figures 8 (a) and (b) indicate that MSAS sequences with two aftershocks have a more significant effect on V_D than MSAS sequences with one aftershock, as presented in Figs. 7 (a) and (b), respectively. The effects of the aftershocks on hysteretic energy in Fig. 8 exhibited an increase from 20% to 40% as the relative intensity, ∇PGA, increased from 0.5 to 0.8.

The aftershock effects on the hysteretic energy cannot be ignored based on the above observations. In particular, the aftershock more significantly influences

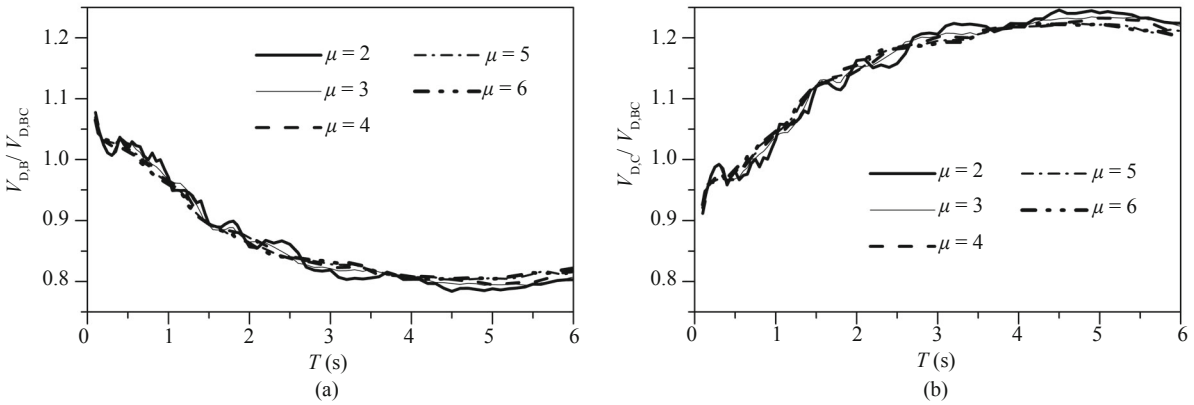

Fig. 6 Mean $V_{D,seq}$ of a given site normalized by mean $V_{D,seq}$ of all site classes for the EPP systems under a set of given conditions (for MSAS sequences with one aftershock, $\zeta = 0.05$, $\nabla PGA = 0.5$ and $\mu = 2$, 3, 4, 5 and 6): (a) site class B; (b) site class C

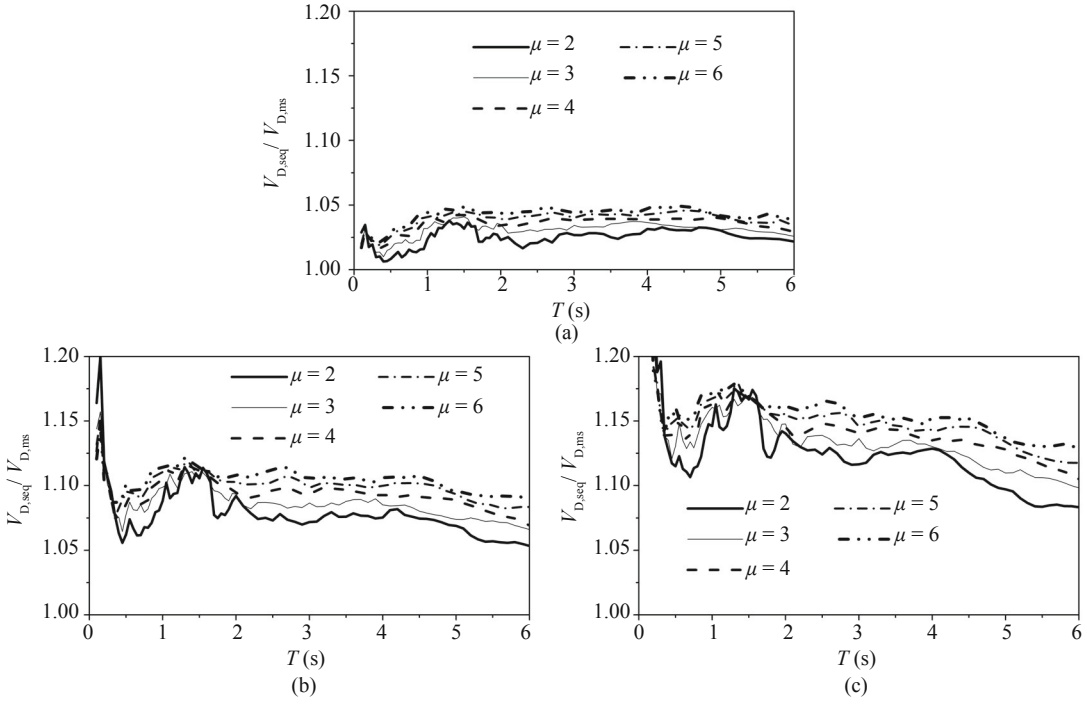

Fig. 7 Mean $V_{D,seq}/V_{D,ms}$ for the EPP systems under a set of given conditions (for MSAS sequences with one aftershock on site Class B, $\zeta = 0.05$ and $\mu = 2$, 3,4,5 and 6) for different values of ∇PGA: (a) $\nabla PGA = 0.5$; (b) $\nabla PGA = 0.8$; (c) $\nabla PGA = 1.0$

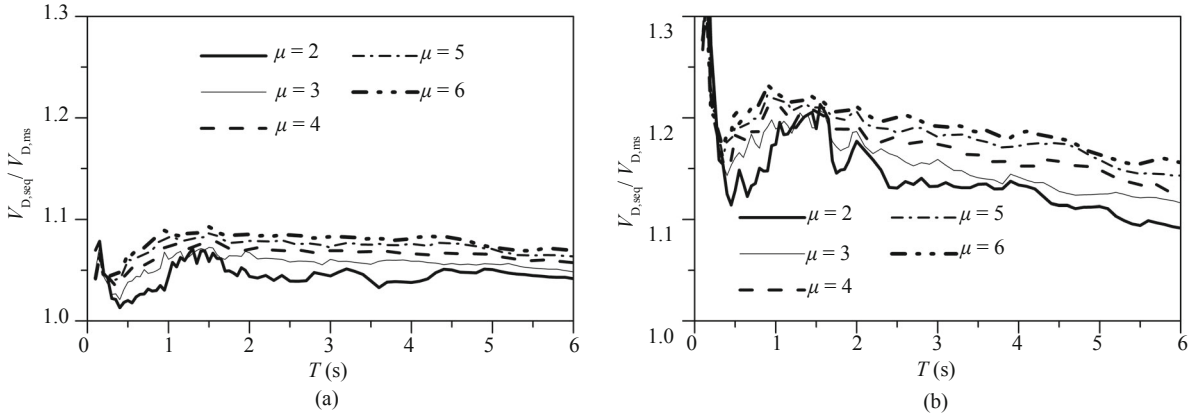

Fig. 8 Mean $V_{D,seq}/V_{D,ms}$ for the EPP systems under a set of given conditions (for MSAS sequences with two aftershocks on site Class B, $\zeta = 0.05$ and $\mu =$ 2, 3, 4, 5 and 6) for different values of ∇PGA: (a) $\nabla PGA = 0.5$; (b) $\nabla PGA = 0.8$

the hysteretic energy of structures with short periods as compared to structures with other periods. The same conclusion is stated in literature (Goda, 2012; Goda and Taylor, 2012; Zhai *et al.*, 2015) for other response measures such as inelastic displacement ratio, peak ductility demand, and strength reduction factor. Compared with the results reported in literature (Goda, 2012; Goda and Taylor, 2012; Zhai *et al.*, 2015), the aftershock has a more significant influence on the hysteretic energy.

4.5 Effect of hysteretic model

The mean $V_{D,seq}$ was analyzed with different models to investigate the effect of the hysteretic models on the mean $V_{D,seq}$. The mean $V_{D,seq}$ for a given hysteretic model in Fig. 9 was normalized with the mean $V_{D,seq}$ of an EPP model under a set of given conditions (for MSAS sequences with one aftershock on site class B, $\zeta = 0.05$, $\nabla PGA = 0.5$ and $\mu = 2$, 3, 4, 5, and 6) for two different hysteretic models.

The $V_{D,seq}$ ratios in Fig. 9 were significantly dependent on the vibration period in the short period range and exhibited sharp decreases with an increase of the vibration period. In the medium and long period range, the ratios of $V_{D,seq}$ were moderately dependent on the vibration period and presented a slow decrease with an increase in the vibration period. This phenomenon indicates that degrading structures with short periods experience a larger hysteretic energy than non-degrading structures and degrading structures with long periods experience a smaller hysteretic energy than

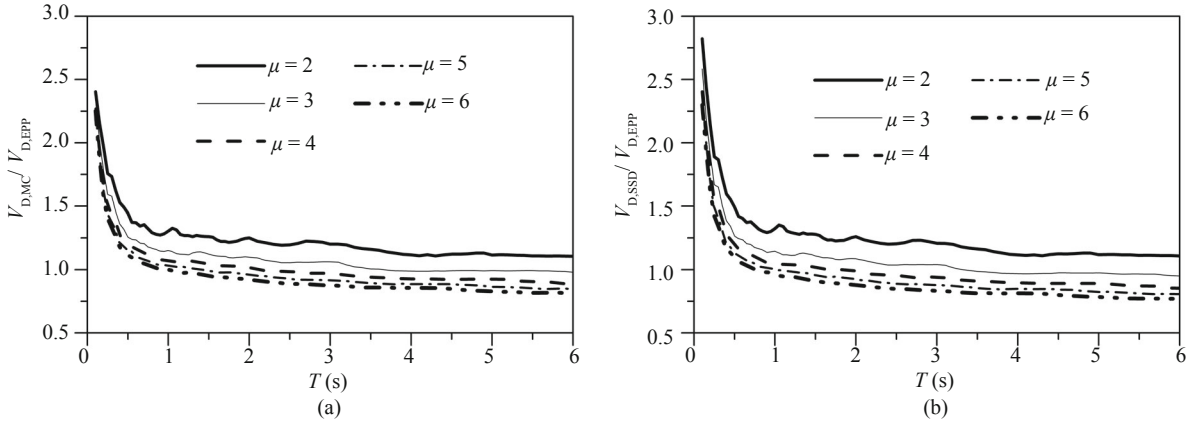

Fig. 9 Mean ratios of $V_{D,seq}$ in each hysteretic model to $V_{D,seq}$ for the EPP systems under a set of given conditions (for MSAS sequences with one aftershock on site Class B, $\zeta = 0.05$, $\nabla PGA = 0.5$ and $\mu = 2$, 3, 4, 5 and 6) for two different hysteretic models: (a) MC model; (b) SSD model

non-degrading structures, all of which was confirmed by recent earthquakes. For example, in the 2010-2011 New Zealand earthquakes (Kam *et al.*, 2011; Jeon *et al.*, 2015), the first aftershock resulted in the column shear failure and column shear cracking of a three-story RC frame building with masonry infill, whereas the second aftershock resulted in the complete collapse of the damaged building. In addition, many masonry structures have collapsed or have been damaged in the earthquake sequences of central Italy (GEER, 2016).

In the short period range, the effects of the structural degrading behaviors were significant for structures with lower ductility values, μ. For example, the maximum ratio of $V_{D,seq}$ corresponding to $\mu = 2$ in Fig. 9 (b) was about 2.8. In the medium-long period region, the ratios of $V_{D,seq}$ varied within the interval of [1.0 1.5]. In the whole period, the $V_{D,seq}$ ratios were dependent on the ductility value, μ, and decreased with an increase in the ductility value, μ. The effects of the models on the ratios of $V_{D,seq}$ were more significant for structures with lower ductility values than for structures with higher ductility values. The influence of the SSD model on $V_{D,seq}$ was more significant than that of the MC model. For example, the maximum effect of the MC model on $V_{D,seq}$ was about 140%, whereas the maximum effect of the SSD model on the $V_{D,seq}$ was about 180%.

4.6 Effect of damping ratio

The $V_{D,seq}$ for an EPP system with a damping ratio, ζ, of 0.02 and 0.1 was calculated to investigate the effects of damping ratios on the mean $V_{D,seq}$. The $V_{D,seq}$ for an EPP system with $\zeta = 0.02$ and 0.1 was then normalized by the $V_{D,seq}$ of an EPP system with $\zeta = 0.05$ for each MSAS sequence. Finally, the mean normalized $V_{D,seq}$ of the MSAS sequences was computed.

Figure 10 presents the variation of the mean normalized $V_{D,seq}$ for the EPP systems under a set of given conditions (for MSAS sequences with one aftershock on site class B, $\nabla PGA = 0.5$ and $\mu = 2$, 3, 4, 5, and 6) for two different damping ratios. The mean normalized $V_{D,seq}$ in Figure 10 (a) was greater than 1.0, while that in Figure 10 (b) was smaller than 1.0. This phenomenon indicates a $V_{D,seq}$ decrease with a damping ratio, ζ, increase.

The majority of the mean normalized $V_{D,seq}$ values in Fig. 10 (a) were smaller than 1.3, and majority of

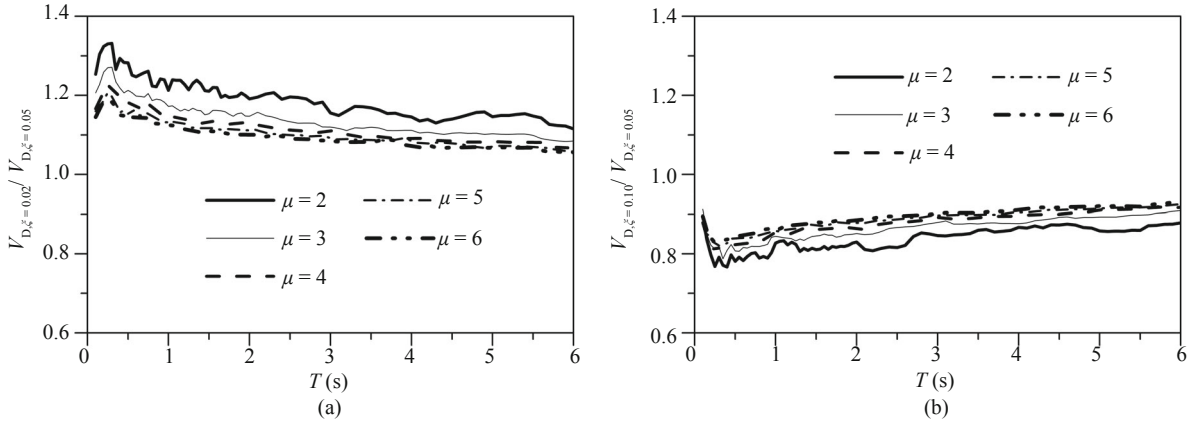

Fig. 10 Mean normalized $V_{D,seq}$ for the EPP systems under a set of given conditions (for MSAS sequences with one aftershock on site Class B, $\nabla PGA = 0.5$ and $\mu = 2$, 3, 4, 5 and 6) for two different damping ratios: (a) $\zeta = 0.02$; (b) $\zeta = 0.1$

the mean normalized $V_{D,seq}$ values in Figure 10 (b) were greater than 0.8. Thus, the maximum error was about 130% when the mean $V_{D,seq}$ with $\zeta = 0.02$ was evaluated using the mean $V_{D,seq}$ with $\zeta = 0.05$. The maximum error was about 80% when the mean $V_{D,seq}$ with $\zeta = 0.1$ was evaluated using the mean $V_{D,seq}$ with $\zeta = 0.05$.

The conclusions in Section 4 are applicable to structures with nonlinear dynamic responses dominated by the fundamental vibration mode. The reliable modification of the results obtained in this manuscript can also be used to evaluate the nonlinear responses of structures higher vibration modes.

5 Prediction equation

Based on the above statements, the mean $V_{D,seq}$ is dependent on the vibration period, damping ratio, and ductility value, μ, of the whole period region. In addition, the relative intensity, ∇PGA, and hysteretic models have an obvious effect on the hysteretic energy of the structures. Furthermore, the hysteretic energy should satisfy the following boundary conditions:

$$V_D(T, \mu = 1) = 0 \tag{15}$$

According to the above discussions and Eq. (15), the hysteretic energy prediction equation can be expressed as follows:

$$V_{D,seq}^{0.1g} = \frac{b_1 \zeta^{0.1} T^{0.3} + b_2 T^{0.45} + b_3 T (\ln \mu)^{-0.3}}{1 + \mu^{1.3} + b_4 T + b_5 T^{b_6} \ln \mu + 0.75 T (\ln \mu)^{b_7}} (\mu - 1) \tag{16}$$

where T is the vibration period and $V_{D,seq}^{0.1g}$ is the mass-normalized hysteretic energy for the benchmark seismic intensity (PGA = 0.1 g). Parameters b_1, b_2, b_3, b_4, b_5, b_6, and b_7 were computed by a nonlinear least-square regression analysis using the Levenberg-Marquardt method (Bates and Watts, 1988).

The prediction equation heavily depended on the inspection of the data and characteristics of the predictive equations. Many tentative parameters were considered in the initial form to determine the final form of Eq. (16). These parameters were modified according to the residuals until a predictive equation was acquired to obtain a good estimation of the mean plus one standard deviation of $V_{D,Seq}$ at different cases. Although the subjective judgment cannot be avoided in this process, it is an efficient method for obtaining a prediction equation with high accuracy and fewer parameters.

The values of b_1, b_2, b_3, b_4, b_5, b_6, and b_7 of the mean plus one standard deviation of $V_{D,seq}$ for the MSAS sequences with one aftershock and two aftershocks are summarized in Tables 3 and 4. Figures 11 and 12 present a comparison between the computed mean plus one standard deviation of $V_{D,seq}$ from Eq. (16) and

Table 3 Site-dependent parameters of mean-plus-one standard deviation of $V_{D,seq}$ to be used in Eq. (16) for MSAS sequences with one aftershock

Relative intensity	Site class	Model	b_1	b_2	b_3	b_4	b_5	b_6	b_7
∇PGA = 0.5	B	EPP	-5.71	7.04	-0.83	-1.11	3.87	0.78	3.54
		MC	-5.88	7.93	-1.11	-1.91	4.97	0.83	4.12
		SSD	-6.17	8.31	-1.14	-2.22	5.67	0.85	4.32
	C	EPP	-3.60	4.60	-0.61	-0.29	-0.19	0.86	2.44
		MC	-3.64	5.22	-0.84	-0.46	0.01	2.55	3.02
		SSD	-4.36	6.06	-0.92	-0.68	0.72	0.96	3.28
∇PGA = 0.8	B	EPP	-6.26	7.69	-0.89	-1.22	4.29	0.81	3.62
		MC	-6.48	8.71	-1.21	-2.16	5.60	0.85	4.23
		SSD	-6.72	8.96	-1.17	-2.51	6.26	0.89	4.41
	C	EPP	-3.77	4.81	-0.60	-0.39	0.01	2.51	2.44
		MC	-4.20	5.90	-0.92	-0.60	0.39	1.10	3.11
		SSD	-4.73	6.52	-0.98	-0.78	0.94	0.97	3.36
∇PGA = 1.0	B	EPP	-6.69	8.22	-0.95	-1.33	4.60	0.83	3.68
		MC	-6.89	9.20	-1.25	-2.32	5.87	0.88	4.28
		SSD	-7.10	9.40	-1.22	-2.61	6.38	0.91	4.45
	C	EPP	-3.93	5.07	-0.70	-0.32	-0.14	0.68	2.49
		MC	-4.45	6.22	-0.97	-0.65	0.49	1.09	3.15
		SSD	-5.01	6.86	-1.02	-0.83	1.05	1.00	3.41

Table 4 Site-dependent parameters of mean-plus-one standard deviation of $V_{D,seq}$ to be used in Eq. (16) for MSAS sequences with two aftershocks

Relative intensity	Site class	Model	b_1	b_2	b_3	b_4	b_5	b_6	b_7
$\nabla PGA = 0.5$	B	EPP	-7.24	8.69	-0.90	-0.80	4.17	0.59	3.41
		MC	-7.31	9.57	-1.18	-1.39	4.62	0.72	3.95
		SSD	-7.59	9.92	-1.19	-1.61	5.14	0.75	4.13
	C	EPP	-5.45	6.50	-0.70	-0.40	0.01	2.93	2.39
		MC	-5.55	7.52	-1.11	-0.59	0.13	1.80	3.04
		SSD	-5.93	8.00	-1.16	-0.72	0.42	1.40	3.24
$\nabla PGA = 0.8$	B	EPP	-9.07	10.81	-1.08	-1.10	5.73	0.65	3.66
		MC	-9.00	11.67	-1.36	-1.92	6.30	0.77	4.23
		SSD	-9.18	11.79	-1.28	-2.17	6.65	0.82	4.38
	C	EPP	-5.95	7.17	-0.83	-0.39	0.01	2.91	2.42
		MC	-6.15	8.37	-1.25	-0.67	0.29	1.52	3.12
		SSD	-6.72	9.00	-1.28	-0.85	0.70	1.29	3.35

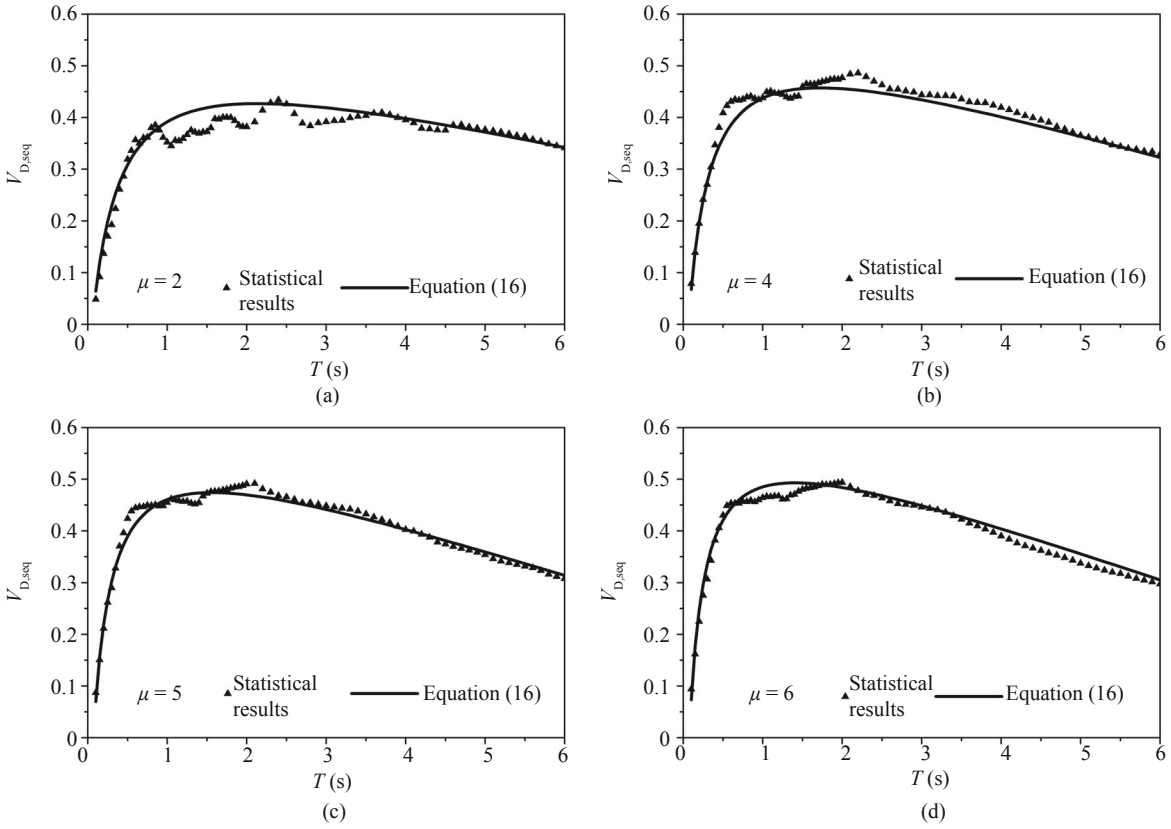

Fig. 11 Comparison of mean-plus-one standard deviation of $V_{D,seq}$ computed using Eq.(16) with the statistical results for the EPP systems under a set of given conditions (for MSAS sequences with one aftershock on site Class B, $\zeta = 0.05$ and $\nabla PGA = 0.5$) for different ductility values: (a) $\mu = 2$; (b) $\mu = 4$; (c) $\mu = 5$; (d) $\mu = 6$

the statistical results of the MSAS sequences with one aftershock on site classes B and C, respectively. In general, the proposed simplified equation in Figs. 11 and 12 provided good estimates of the mean plus one standard deviation of $V_{D,seq}$.

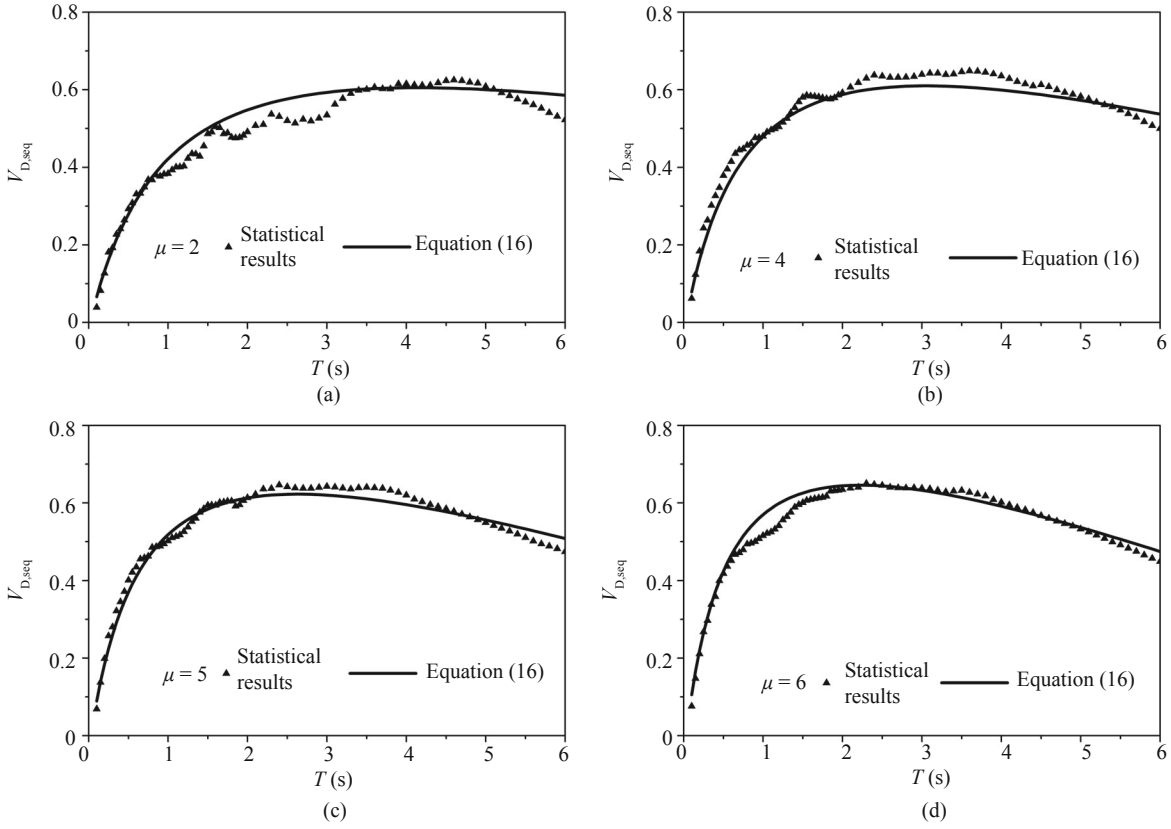

Fig. 12 Comparison of mean-plus-one standard deviation of $V_{D,seq}$ computed using Eq.(16) with the statistical results for the EPP systems under a set of given conditions (for MSAS sequences with one aftershock on site Class C, $\zeta = 0.05$ and $\nabla PGA = 0.5$) for different ductility values: (a) $\mu = 2$; (b) $\mu = 4$; (c) $\mu = 5$; (d) $\mu = 6$

6 Conclusions

The present study evaluated the hysteretic energy of SDOF structures subjected to MSAS sequences. The hysteretic energy of the MSAS sequences was normalized by mass, m, and was expressed in terms of the equivalent velocity, $V_{D,seq}$. The variation of the equivalent velocity, $V_{D,seq}$, was studied for consideration of the ductility values, site conditions, relative intensities, number of aftershocks, hysteretic models, and damping ratios. The equivalent velocity was computed for the MSAS sequences and subsequent statistical studies were performed. The following conclusions were drawn from the investigation:

1. The mean $V_{D,seq}$ for the EPP systems increased following an increase of the vibration period in the short period range, though significant changes were not observed in the vibration period of the medium-long period range. In the long period range, the mean $V_{D,seq}$ of the EPP systems decreased with an increase of the vibration period. The mean $V_{D,seq}$ was dependent upon the ductility value, μ, and increased with an increase in the ductility value, μ, except for lower ductility values (i.e., $\mu = 2$, 3) in the long period range.

2. The coefficients of variation (COVs) significantly changed with vibration period changes in the whole period range. The COV varied from 0.2–0.3 to 0.8–0.9 in the period range, which is meaningful for engineering structures. The COVs of the $V_{D,seq}$ for different site classes of MSAS sequences with one aftershock exhibited a similar trend. The effect of the ductility value, μ, on the COVs changed with the vibration period.

3. The effects of the site conditions on $V_{D,seq}$ was negligible in the short-medium period range. In the long period range, the effects of the site conditions on $V_{D,seq}$ was high. The overall error reached 25% in the long period range if the mean $V_{D,seq}$ for all site classes was employed to estimate $V_{D,seq}$ for a given site. Note that results in this study are not applicable to structures on soft soil and rock.

4. The aftershock ground motions increased $V_{D,seq}$ as compared to cases that solely consider the mainshock ground motion. As the ∇PGA increased from 0.5 to 1.0 for MSAS sequences with one aftershock, the effects of the aftershocks on the $V_{D,seq}$ and hysteretic energy, $E_{H,seq}$, generally increased from 5% to 15% and 10% to 30%, respectively. As the PGA_{as}/PGA_{ms} increased from 0.5 to 0.8 for MSAS sequences with two aftershocks, the aftershock effects on $V_{D,seq}$ and the hysteretic energy, $E_{H,seq}$, increased from 10% to 20% and 20% to 40%, respectively.

5. Degrading structures with lower ductility values produced more hysteretic energy than non-degrading structures with lower ductility values when subjected to

MSAS sequences. The effects of the hysteretic models on $V_{D,seq}$ were more significant in the short period range than in other period ranges. The mean $V_{D,seq}$ for the EPP systems decreased with an increase of the damping ratio, ζ.

6. The present study proposed a prediction expression for $V_{D,seq}$ as a function of the vibration period, ductility value, and damping ratio. A comparison was executed between the computed $V_{D,seq}$ using the proposed expression and the exact $V_{D,seq}$ for EPP systems subjected to MSAS sequences with one aftershock. The computed results agree well with the statistical results.

The MSAS sequences were only selected for three earthquakes (Imperial Valley, Northridge, and Chi Chi) due to recorded MSAS sequence limitations. Therefore, the conclusions given in this manuscript may not be suitable for regions that may exhibit different earthquake mechanisms from these three regions.

Acknowledgement

This investigation is supported by the National Key R&D Program of China (2017YFC1500602, 2016YFC0701108), the National Natural Science Foundation of China (No. 51322801, 51708161), the Outstanding Talents Jump Promotion Plan of Basic Research of Harbin Institute of Technology, China Postdoctoral Science Foundation (No. 2016M601430). These supports are greatly appreciated.

References

Akiyama H (1985), *Earthquake-Resistant Limit State Design for Buildings*, University of Tokyo Press.

Amiri GG, Darzi GA and Amiri JV (2008), "Design Elastic Input Energy Spectra Based on Iranian Earthquakes," *Canadian Journal of Civil Engineering*, **35**(6): 635–646.

Arroyo D and Ordaz M (2007a), "Hysteretic Energy Demands for SDOF Systems Subjected to Narrow Band Earthquake Ground Motions. Applications to the Lake Bed Zone of Mexico City," *Journal of Earthquake Engineering*, **11**(2): 147–165.

Arroyo D and Ordaz M (2007b), "On the Estimation of Hysteretic Energy Demands for SDOF Systems," *Earthquake Engineering and Structural Dynamics*, **36**(15): 2365–2382.

Augenti N and Parisi F (2010), "Learning from Construction Failures due to the 2009 L'Aquila, Italy, Earthquake," *Journal of Performance of Constructed Facilities*, **24**(6): 536–555.

Ay BÖ and Akkar S (2012), "A Procedure on Ground Motion Selection and Scaling for Nonlinear Response of Simple Structural Systems," *Earthquake Engineering and Structural Dynamics*, **41**(12): 1693–1707.

Baker JW (2010), "Conditional Mean Spectrum: Tool for Ground-motion Selection," *Journal of Structural Engineering*, **137**(3): 322–331.

Baker JW and Allin Cornell C (2006), "Spectral Shape, Epsilon and Record Selection," *Earthquake Engineering and Structural Dynamics*, **35**(9): 1077–1095.

Bates DM and Watts DG (1988), *Nonlinear Regression Analysis and Its Applications*, Wiley, New York.

Benavent-Climent A, López-Almansa F and Bravo-González DA (2010), "Design Energy Input Spectra for Moderate-to-high Seismicity Regions Based on Colombian Earthquakes," *Soil Dynamics and Earthquake Engineering*, **30**(11): 1129–1148.

Benavent-Climent A, Pujades LG and López-Almansa F (2002), "Design Energy Input Spectra for Moderate-seismicity Regions," *Earthquake Engineering and Structural Dynamics*, **31**(5): 1151–1172.

Bojórquez E, Reyes-Salazar A, Terán-Gilmore A and Ruiz SE (2010), "Energy-Based Damage Index for Steel Structures," *Steel and Composite Structures*, **10**(4): 343–360.

Bojórquez E, Ruiz SE and Terán-Gilmore A (2008), "Reliability-Based Evaluation of Steel Structures using Energy Concepts," *Engineering Structures*, **30**(6): 1745–1759.

Boore DM (1993), "Some Notes Concerning the Determination of Shear-wave Velocity and Attenuation," *Proceedings of Geophysical Techniques for Site and Material Characterization*, 129–134.

Ceci AM, Contento A, Fanale L, Galeota D, Gattulli V, Lepidi M and Potenza F (2010), "Structural Performance of the Historic and Modern Buildings of the University of L'Aquila During the Seismic Events of April 2009," *Engineering Structures*, **32**(7): 1899–1924.

CEN (2003), *Eurocode 8: Design of Structures for Earthquake Resistance, part 1: General Rules, Seismic Actions and Rules for Buildings*, European Committee for Standardization, Brussels.

CENC (2008), China Earthquake Networks Center, (http://data.earthquake.cn and http://www.csndmc.ac.cn).

Chai YH and Fajfar P (2000), "A Procedure for Estimating Input Energy Spectra for Seismic Design," *Journal of Earthquake Engineering*, **4**(4): 539–561.

Chai YH, Fajfar P and Romstad KM (1998), "Formulation of Duration-Dependent Inelastic Seismic Design Spectrum," *Journal of Structural Engineering*, **124**(8): 913–921.

Chai YH, Romstad KM and Bird SM (1995), "Energy-Based Linear Damage Model for High-Intensity Seismic Loading," *Journal of Structural Engineering*,**121**(5): 857–864.

Choi H and Kim J (2006), "Energy-Based Seismic Design of Buckling-Restrained Braced Frames using Hysteretic Energy Spectrum," *Engineering Structures*, **28**(2): 304-311.

Decanini LD and Mollaioli F (1998), "Formulation of Elastic Earthquake Input Energy Spectra," *Earthquake Engineering and Structural Dynamics*, **27**(12): 1503–1522.

Decanini LD and Mollaioli F (2001), "An Energy-Based Methodology for the Assessment of Seismic Demand," *Soil Dynamics and Earthquake Engineering*, **21**(2): 113–137.

Dindar AA, Yalçın C, Yüksel E, Özkaynak H and Büyüköztürk O (2015), "Development of Earthquake Energy Demand Spectra," *Earthquake Spectra*, **31**(3): 1667–1689.

Di Sarno L (2013), "Effects of Multiple Earthquakes on Inelastic Structural Response," *Engineering Structures*, **54**: 673–681.

Di Sarno L, Yenidogan C and Erdik M (2013), "Field Evidence and Numerical Investigation of the M_W = 7.1 October 23 Van, Tabanlı and the M_W > 5.7 November Earthquakes of 2011," *Bulletin of Earthquake Engineering*, **11**(1): 313–346.

Dong Y and Frangopol DM (2015), "Risk and Resilience Assessment of Bridges under Mainshock and Aftershocks Incorporating Uncertainties," *Engineering Structures* **83**: 198–208.

Faisal A, Majid TA and Hatzigeorgiou GD (2013), "Investigation of Story Ductility Demands of Inelastic Concrete Frames Subjected to Repeated Earthquakes," *Soil Dynamics and Earthquake Engineering*, **44**: 42–53.

Fajfar P and Vidic T (1994), "Consistent Inelastic Design Spectra: Hysteretic and Input Energy," *Earthquake Engineering and Structural Dynamics*, **23**(5): 523–537.

GEER (2016), Geotechnical Extreme Events Reconnaissance, (http://geerassociation.org/component/geer_reports /?view=geerreports&id=76&layout=default).

Goda K (2012), "Nonlinear Response Potential of Mainshock-Aftershock Sequences from Japanese Earthquakes," *Bulletin of the Seismological Society of America*, **102**(5): 2139–2156.

Goda K and Taylor CA (2012), "Effects of Aftershocks on Peak Ductility Demand Due to Strong Ground Motion Records from Shallow Crustal Earthquakes," *Earthquake Engineering and Structural Dynamics*, **41**(15): 2311–2330.

Gong Y, Xue Y, Xu L and Grierson DE (2012), "Energy-Based Design Optimization of Steel Building Frameworks Using Nonlinear Response History Analysis," *Journal of Constructional Steel Research*, **68**(1): 43–50.

Hatzigeorgiou GD (2010a), "Behavior Factors for Nonlinear Structures Subjected to Multiple Near-Fault Earthquakes," *Computers and Structures*, **88**(5-6): 309–321.

Hatzigeorgiou GD (2010b), "Ductility Demand Spectra for Multiple Near-And Far-Fault Earthquakes," *Soil Dynamics and Earthquake Engineering*, **30**(4): 170–183.

Hatzigeorgiou GD and Liolios AA (2010), "Nonlinear Behaviour of RC Frames under Repeated Strong Ground Motions," *Soil Dynamics and Earthquake Engineering*, **30**(10): 1010–1025.

Housner GW (1956), "Limit Design of Structures to Resist Earthquakes," *Proceedings of First World Conference on Earthquake Engineering*, **5**: 1-12.

International Building Code (IBC) (2006), International Code Council Inc., 4051 West Flossmoor Road, Country Club Hills.

Jeon JS, DesRoches R, Lowes LN and Brilakis I (2015), "Framework of Aftershock Fragility Assessment–Case Studies: Older California Reinforced Concrete Building Frames," *Earthquake Engineering and Structural Dynamics*, **44**(15): 2617–2636.

Kam WY, Pampanin S and Elwood K (2011), "Seismic Performance of Reinforced Concrete Buildings in the 22 February Christchurch (Lyttelton) Earthquake," *Bulletin of the New Zealand Society for Earthquake Engineering*, **44**(4): 239–278.

Katsanos EI, Sextos AG, and Manolis GD (2010), "Selection of Earthquake Ground Motion Records: A State-of-the-Art Review From A Structural Engineering Perspective," *Soil Dynamics and Earthquake Engineering*, **30**(4): 157–169.

Kunnath SK, Reinhorn AM and Park YJ (1990), "Analytical Modeling of Inelastic Seismic Response of R/C Structures," *Journal of Structural Engineering*, **116**(4): 996–1017.

Kunnath SK, Reinhorn AM and Lobo RF (1992), "IDARC Version3.0: A Program For the Inelastic Damage Analysis of Reinforced Concrete Structures," *Technical Report No. NCEER-92-0022*, National Center for Earthquake Engineering Research, State University of New York, Buffalo.

Kuwamura H and Galambos TV (1989), "Earthquake Load for Structural Reliability," *Journal of Structural Engineering*, **115**(6): 1446–1462.

Kyoshin-Net (2009), National Research Institute for Earth Science and Disaster Resilience, *http://www.kyoshin.bosai.go.jp*.

López-Almansa F, Yazgan AU and Benavent-Climent A (2013), "Design Energy Input Spectra for High Seismicity Regions Based on Turkish Registers," *Bulletin of Earthquake Engineering*, **11**(4): 885–912.

Manfredi G (2001), "Evaluation of Seismic Energy Demand," *Earthquake Engineering and Structural Dynamics*, **30**(4): 485–499.

Miranda E and Ruiz-Garcia J (2002), "Influence of Stiffness Degradation on Strength Demands of Structures Built on Soft Soil Sites," *Engineering Structures*, **24**(10): 1271–1281.

Moustafa A and Takewaki I (2010), "Modeling Critical Ground-Motion Sequences for Inelastic Structures,"

Advances in Structural Engineering, **13**(4): 665–680.

Moustafa A and Takewaki I (2011), "Response of Nonlinear Single-Degree-of-Freedom Structures to Random Acceleration Sequences," *Engineering Structures*, **33**(4): 1251–1258.

Nazari N, van de Lindt JW and Li Y (2013), "Effect of Mainshock-Aftershock Sequences on Woodframe Building Damage Fragilities," *Journal of Performance of Constructed Facilities*, **29**(1): 04014036.

Rahnama M and Krawinkler H (1993), "*Effects of Soft Soil And Hysteresis Model On Seismic Demands*," John A. Blume Earthquake Engineering Center, chapter 3, pp 36–37.

Riddell R and Garcia JE (2001), "Hysteretic Energy Spectrum and Damage Control," *Earthquake Engineering and Structural Dynamics*, **30**(12): 1791–1816.

Ruiz-García J and Negrete-Manriquez JC (2011), "Evaluation of Drift Demands in Existing Steel Frames under As-Recorded Far-Field and Near-Fault Mainshock-aftershock Seismic Sequences," *Engineering Structures*, **33**(2): 621–634.

Uang CM and Bertero VV (1990), "Evaluation of Seismic Energy in Structures," *Earthquake Engineering and Structural Dynamics*, **19**(1): 77–90.

Zahrah TF and Hall WJ (1982), *Seismic Energy Absorption in Simple Structures*, Structural Research Series no. 501, University of Illinois, Urbana.

Zhai CH, Ji DF,Wen WP, Lei WD, Xie LL and Gong MS (2016), "The Inelastic Input Energy Spectra for Main Shock–Aftershock Sequences," Earthquake Spectra, **32**(4): 2149–2166.

Zhai CH, Wen WP, Chen ZQ, Li S and Xie LL (2013a), "Damage Spectra for the Mainshock-Aftershock Sequence-Type Ground Motions," *Soil Dynamics and Earthquake Engineering*, **45**: 1–12.

Zhai CH, Wen WP, Li S and Xie LL (2014), "The Damage Investigation of Inelastic SDOF Structure under the Mainshock-Aftershock Sequence-Type Ground Motions," *Soil Dynamics and Earthquake Engineering*, **59**: 30–41.

Zhai CH, Wen WP, Li S and Xie LL (2015), "The Ductility-Based Strength Reduction Factor for the Mainshock-aftershock Sequence-type Ground Motions," *Bulletin of Earthquake Engineering*, **13**(10): 2893–2914.

Zhai CH, Wen WP, Zhu TT, Li S and Xie LL (2013b), "Inelastic Displacement Ratios for Design of Structures with Constant Damage Performance," *Engineering Structures*, **52**: 53–63.